Transport of polydisperse colloid suspensions in a single fracture

DATASET *in* WATER RESOURCES RESEARCH · NOVEMBER 2013

Impact Factor: 3.55

2 AUTHORS:

Scott C James
Baylor University
118 PUBLICATIONS **584** CITATIONS
SEE PROFILE

Constantinos V. Chrysikopoulos
Technical University of Crete
143 PUBLICATIONS **2,004** CITATIONS
SEE PROFILE

WATER RESOURCES RESEARCH, VOL. 35, NO. 3, PAGES 707–718, MARCH 1999

Transport of polydisperse colloid suspensions in a single fracture

Scott C. James and Constantinos V. Chrysikopoulos

Department of Civil and Environmental Engineering, University of California, Irvine

Abstract. The transport of variably sized colloids (polydisperse) in a fracture with uniform aperture is investigated by a particle-tracking model that treats colloids as discrete particles with unique transport properties while accounting for either matrix diffusion or irreversible colloid deposition. For the special case of a monodisperse colloid suspension the particle-tracking model is in perfect agreement with predictions based on an existing analytical solution. It is shown that lognormal colloid size distributions exhibit greater spreading than monodisperse suspensions. Increasing the fracture porosity of the solid matrix leads to higher matrix diffusion, which in turn delays particle breakthrough for both the monodisperse and variably sized colloid suspensions. The smallest particles of a distribution are more greatly affected by matrix diffusion whereas the largest particles are transported faster and further along a fracture. Both perfect sink and kinetic colloid deposition onto fracture surfaces are examined. Kinetic deposition accounts for colloid surface exclusion by either a linear or nonlinear blocking function. For both cases the smallest colloid particles tend to preferentially deposit onto the fracture wall. Both matrix diffusion and surface deposition tend to discretize colloid distributions according to particle size so that larger particles are least retarded and smaller particles are more slowly transported. Furthermore, it is shown that the rate of colloid deposition is inversely proportional to the fracture aperture.

1. Introduction

Groundwater flow and contaminant transport in fractured media have been the focus of several studies [e.g., *Grisak and Pickens*, 1981; *Neretnieks et al*., 1982; *Johns and Roberts*, 1991; *Keller et al*., 1995; *Berkowitz and Scher*, 1995; *Berkowitz and Zhou*, 1996; *Zimmerman and Bodvarsson*, 1996] because the possibility for significant environmental contamination by harmful radioactive waste, which is often disposed of in fractured geologic repositories, is an area of increasing concern [*Yamashita and Kimura*, 1990]. Furthermore, contamination of fractured subsurface formations by organic as well as inorganic toxins and the role of colloids in enhancing or diminishing contaminant transport have increasingly captured the interest of researchers [*Smith and Degueldre*, 1993]. For instance, the Swiss program, Project Gewahr [*Statens Karnkraftinspektion* (*SKI*), *Swedish Nuclear Power Inspectorate*, 1991], which aimed to demonstrate the feasibility of deep disposal of radioactive waste in bedrock, improved current understanding of flow and transport of both contaminants and colloids in fractured media. *Smith and Degueldre* [1993] found that depending on environmental conditions (e.g., hydrodynamics or contaminant and colloid sorption characteristics), colloids could both enhance and diminish contaminant transport and significantly affect contaminant migration.

Studies of colloid transport in a single fracture have been reported by *Abdel-Salam and Chrysikopoulos* [1995a, b], where it was demonstrated that the dispersion of colloids and solutes sorbed onto colloids (cotransport) is enhanced by fracture wall roughness. The attachment of colloids in parallel plate systems has been examined by *Adamczyk et al*. [1983] and in a single fracture has been examined by *Abdel-Salam and Chrysikopoulos* [1994]. *Ibaraki and Sudicky* [1995] have developed a comprehensive model analyzing monodisperse colloid-facilitated contaminant transport in discretely fractured porous media. Their two-dimensional numerical model incorporated advective-dispersive aqueous phase solute transport in the fractures and the porous matrix, colloid transport in the fractures, and both equilibrium and kinetic sorption of the contaminant. Much of the research performed to date on colloid transport is based on uniform particles (monodisperse colloid suspensions). However, it should be noted that in natural systems, colloid particles can range over several orders of magnitude in diameter (polydisperse).

Colloids are very fine particles such as clay minerals, metal oxides, viruses, bacteria, and organic macromolecules that range in size from 10^{-3} to 10 μm [*Chrysikopoulos and Sim*, 1996]. A wide variety of microorganisms, organic, and inorganic colloidal material can be found in groundwater. Colloids are naturally present in groundwater or artificially introduced through injection of cementing as well as slurry agents or during well installation and operation. Colloids, both in the liquid phase and attached to solid surfaces, have high specific surface areas per unit mass ($\sim$300 m^2/g^{-1} [*Chung and Lee*, 1992]); thus they possess a high sorptive capacity for contaminants and are themselves able to sorb onto solid surfaces. Colloid transport differs from solute transport because of colloidal particle interactions (e.g., flocculation), mechanical clogging effects, and surface reactions (e.g., attachment). The adsorption process of colloids onto solid surfaces is often termed as deposition, attachment, or filtration. Deposition of colloids is generally affected by Brownian motion, the repulsive electric double layer, attractive van der Waals forces, and solution

Paper number 1998WR900059.
0043-1397/99/1998WR900059$09.00

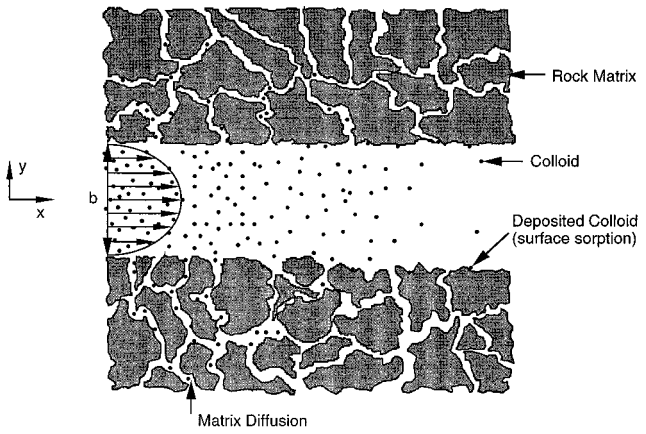

Figure 1. Schematic illustration of a fracture with uniform aperture and a migrating plume of colloids undergoing surface sorption and matrix diffusion. Note that $y = 0$ at the center of the aperture.

chemistry [*Payatakes et al*., 1974]. Particle deposition is also affected by whether fracture surfaces are clean or whether deposition occurs onto previously deposited particles. Detachment of colloids is not expected in fractures where flow velocities are low. *Bowen and Epstein* [1979] have shown experimentally that the release rate of deposited colloids from a smooth parallel plate channel is negligible, and in many studies, colloid deposition is considered irreversible [*Elimelech et al*., 1995; *Johnson et al*., 1996].

In this work, theoretical investigations based on particle-tracking simulations are undertaken to gain a better understanding of the effect of size distribution on colloidal transport in a single fracture. Lognormal colloid diameter distributions are used because they are realistic representations of naturally occurring colloid suspensions [*Ledin et al*., 1994]. Results are compared to an analytical solution available in the literature for monodisperse particle transport within two infinitely long parallel plates. The spreading of polydisperse colloid suspensions is compared to that of a monodisperse suspension. Matrix diffusion, which can serve to increase colloid residence time by back diffusion into the fracture once the bulk of the colloid cloud has moved downstream, can play an important role in colloid transport as well. The effect of matrix diffusion on polydisperse colloid distributions is examined. Furthermore, the effects of particle deposition on the transport of colloids are investigated by perfect sink and kinetic sorption models. For the kinetic sorption case both linear and nonlinear irreversible dynamic blocking functions (DBFs) are employed, first applied to models of colloid transport in fractures by *Chrysikopoulos and Abdel-Salam* [1997]. Finally, the effect of fracture aperture on polydisperse colloid transport is investigated.

2. Model Development

2.1. Flow and Transport

In order to simplify the development of the particle-tracking model a single fracture with uniform aperture, as shown in Figure 1, is considered in this work. Flow in a uniform fracture can be idealized as Poiseuille flow (i.e., having a parabolic velocity profile), where particles can be both advected along the velocity gradient and dispersed because of molecular diffusion [*Buckley and Loyalka*, 1994]. The magnitude of the advective force is a function of the distance from the center of the fracture, the y location. The parabolic velocity profile within a smooth fracture is given by [*Fox and McDonald*, 1992, p. 325]:

$$U_x(y) = U_{\max}\left[1 - 4\left(\frac{y}{b}\right)^2\right] \tag{1}$$

where $U_{\max}$ is the maximum velocity occurring along the centerline, and b is the fracture aperture width. Colloids are assumed to be hard spherical particles (i.e., no surface charge) which are advected and diffused through the aperture and are allowed to penetrate the surrounding matrix by diffusion or attach to fracture walls. Although settling rates can affect colloid transport in fractures, gravitational effects have been disregarded in the interest of simplicity and in order to explicitly examine ideal particle transport in a single uniform fracture. *Ledin et al*. [1994] reported that colloids found in natural environments usually follow a lognormal size distribution. Such a distribution can be mathematically expressed as [*Gelhar*, 1993, p. 19]:

$$\mathcal{N}(d_p) = \frac{\mathcal{N}_o}{\sqrt{2\pi}\zeta d_p}\exp\left[-\tfrac{1}{2}\left(\frac{\ln d_p - \lambda}{\zeta}\right)^2\right] \tag{2}$$

where $\mathcal{N}(d_p)$ is the number of colloids of a given diameter d_p, $\mathcal{N}_o$ is the total number of colloids present in the system, λ is the mean of the log-colloid diameter, and ζ^2 is the variance of the log-colloid diameter. Furthermore, in this work the mean colloid diameter is represented by $\mu = \exp[\lambda + 0.5\zeta^2]$, and the variance of the colloid diameter is represented by $\sigma^2 = \mu^2(e^{\zeta^2} - 1)$ [*Ang and Tang*, 1975].

An analytical solution to monodisperse particle transport in a fracture exists. Assuming that axial advection and transverse diffusion are the important transport mechanisms and that the colloids have had sufficient residence time to establish Taylor dispersion conditions, the advective and diffusive transport forces can be combined to determine the Taylor dispersion coefficient in a parallel plate channel [*Berkowitz and Zhou*, 1996]. The equation relating the spreading of a colloid plume to the average flow velocity, $2U_{\max}/3$, is given by the following diffusion equation [*Buckley and Loyalka*, 1994]

$$\frac{\partial n(x', t)}{\partial t} = D^* \frac{\partial^2 n(x', t)}{\partial x'^2} \tag{3}$$

where n is the temporally and spatially varying particle number density, $x' = x + \frac{2}{3}U_{\max}t$ is the distance from the center of mass of the colloid plume at time t, and D^* is the Taylor dispersion coefficient (which is not a physical constant but depends on the flow and its properties) defined as [*Keller et al*., 1995; *Edwards et al*., 1991]

$$D^* = \mathcal{D} + \frac{2}{945}\frac{U_{\max}^2 b^2}{\mathcal{D}} \tag{4}$$

where $\mathcal{D}$ is the molecular diffusion coefficient of a colloid particle in the fracture described by the Stokes-Einstein equation [*Bird et al*., 1960, p. 514]

$$\mathcal{D} = \frac{kT}{3\pi\eta d_p} \tag{5}$$

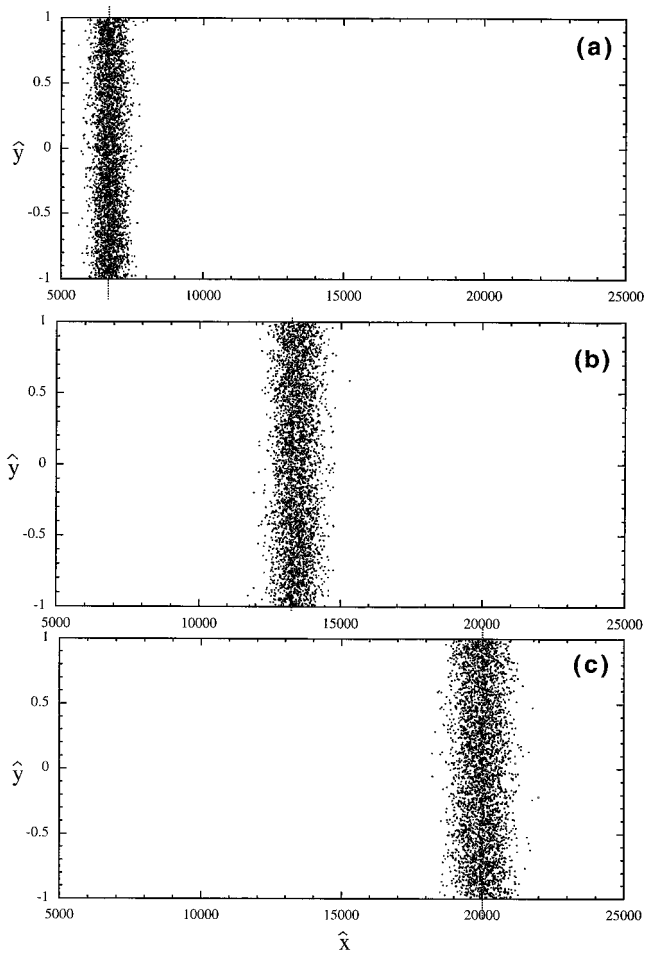

Figure 2. Taylor dispersion in a fracture with uniform aperture at simulation times of (a) 1×10^9, (b) 2×10^9, and (c) 3×10^9 s (here $U_{\max} = 1 \times 10^{-9}$ m s^{-1}). Note that nondimensional coordinates are used.

where k is the Boltzmann's constant, T is the absolute temperature of the solvent, and η is the dynamic viscosity of the solvent. The analytical solution to the diffusion equation, (3), subject to no flux conditions both at the fracture walls and at the centerline, with an instantaneous pulse injection under smooth interstitial flow, is derived by *Taylor* [1953],

$$n(x, t) = \frac{n_o}{(4\pi D^* t)^{1/2}} \exp\left[- \frac{(x - \frac{2}{3} U_{\max} t)^2}{4\pi D^* t} \right] \tag{6}$$

where n_o is the initial particle number concentration at time zero. Although the parabolic velocity profile creates fluid shear in the y direction, the expression for the colloid number concentration is independent of y. Under fully developed Taylor conditions, axial convection and radial diffusion contribute to the overall dispersion with the net result of having the colloids travel in an apparent plug flow. The difference between a parabolic velocity profile and a uniform velocity profile on particle transport lies in the spreading of the colloids. In plug flow the diffusion coefficient $\mathcal{D}$ may be orders of magnitude less than in parabolic flow where the Taylor dispersion coefficient D^* governs the spreading. Figure 2 shows three particle snapshots created by the particle-tracking model for a fracture with aperture 100 μm and maximum fluid velocity 1 nm s^{-1}. The very small fluid velocity, 1 nm s^{-1}, was chosen in order to make more prominent the dispersive effects on the line source of colloids at this scale. It is evident from Figure 2 that the colloids are, on average, traveling with the mean fluid velocity (dashed vertical line). Although there is a parabolic velocity profile within the fracture, the colloids are traveling as if under plug flow conditions because at fully developed Taylor conditions the dispersive pattern of colloids appears to be similar to that observed in plug flow.

2.2. Matrix Diffusion

Diffusion within the matrix is typically modeled as a Fickian process where the concentration gradient is controlling mass transfer. As a colloid moves between fracture and matrix, a sharp gradient is encountered both in porosity and diffusivity. *Thompson and Gelhar* [1990] note that additional deterministic velocity terms are necessary to add to the particle-tracking equations when gradients in diffusivity or porosity exist. The appropriate mathematical expressions are

$$U_{\mathcal{D}} = \nabla \cdot \mathcal{D} \tag{7}$$

$$U_\theta = \mathcal{D}(\nabla \cdot \ln \theta) \tag{8}$$

where $U_{\mathcal{D}}$ and U_θ are the deterministic velocities due to diffusivity and porosity gradients, respectively, and θ is the local porosity. If (7) and (8) are not included in the particle-tracking equations, particles will falsely accumulate in stagnant and low-porosity zones of the flow system.

2.3. Colloid Deposition

2.3.1. Perfect sink approximation. Colloid deposition onto fracture surfaces is often considered a relatively fast process when compared to the groundwater velocity so that a sorption relationship like the Smulochowski-Levich approximation can be assumed valid. The Smulochowski-Levich relationship is an approximate analytical solution to the perfect sink model which solves the transport and continuity equations on the basis of Eulerian theory. With some manipulation it can be cast in a form similar to a linear local equilibrium deposition representation. As opposed to Lagrangian methods where the trajectories of individual particles are calculated (e.g., the particle-tracking method), Eulerian methods describe particles collectively in terms of their distribution, or probability density, in space and time, $n(x, t)$. In any equilibrium analysis the number of sorbed particles per unit fracture surface area, $n^*(x, t)$, is a function of the number of particles in the bulk solution; that is,

$$n^*(x, t) = K_d n(x, t) \tag{9}$$

where K_d is an approximation to the linear equilibrium sorption coefficient. In the Smulochowski-Levich sorption relationship, deposition is described in terms of the particle flux onto sorbent surfaces as a function of the colloid number concentration n, flow velocity $U_{\max}$, molecular diffusion coefficient $\mathcal{D}$, fracture aperture b, and distance from the fracture inlet, x. Because of the lack of detailed information on actual fracture conditions and questionable validity of available colloidal force expressions applicable near walls, the attachment process of colloids is often represented by highly idealized models which, in Eulerian analysis, are employed as boundary conditions for the governing transport equations. The Smulochowski-Levich approximation is a perfect sink model which assumes that the

particle wall hydrodynamic repulsive interaction is exactly counterbalanced by van der Waals attractions between the particle and the wall and that all other colloidal and external forces are absent [*Elimelech et al*., 1995, p. 100]. In view of this approximation an analytically derived expression for the local dimensionless mass transfer coefficient, representing colloid deposition onto the surfaces of a fracture during colloid transport, is defined as [*Adamczyk et al*., 1983]

$$Sh = \frac{Jd_p}{2n\mathcal{D}} \tag{10}$$

where Sh is the Sherwood number, and J is the normal component of the local colloid flux at the wall. *van de Ven* [1989, p. 273] has presented Sherwood numbers for several flow geometries with surface sorption. Specifically, in the case of a parallel plate channel the Sherwood number is given as

$$Sh = 0.538 \left(\frac{bPe}{x}\right)^{1/3} \tag{11}$$

where the fracture Peclet number Pe for a parallel plate aperture is defined as [*Adamczyk and van de Ven*, 1980]

$$Pe = \frac{U_{\max} d_p^3}{2b^2\mathcal{D}} \tag{12}$$

Equating (10) and (11) and subsequently employing (12) yields the following expression for the colloid flux at each surface of the fracture:

$$J = 0.854 \left(\frac{\mathcal{D}^2 U_{\max}}{xb}\right)^{1/3} n(x, t) \tag{13}$$

From the concentration of colloids per unit element of the fracture it is possible to determine the particle flux at any location x on the collector surface in particles per square meter per second because $\mathcal{D}$, $U_{\max}$, and b are known constants. As the particle-tracking code necessitates the use of a discrete time step, the fraction of colloids in solution that is sorbed at each time step can be cast in the form of a linear equilibrium sorption coefficient by relating it to the Smulochowski-Levich approximation,

$$K_d = 0.854 \left(\frac{\mathcal{D}^2 U_{\max}}{xb}\right)^{1/3} \Delta t \tag{14}$$

where Δt is the time step used in the particle-tracking analysis. The preceding expression is employed in (9).

It should be noted that with the use of the Smulochowski-Levich assumptions the fracture walls act as perfect sinks and equilibrium deposition of colloids onto a smooth parallel plate channel can only be approximated. In this particle-tracking model the effect of colloid size variations are accounted for by the flux relationship (13) which is a function of the diffusion coefficient and, consequently, a function of the colloid diameter.

2.3.2. Kinetic relationship. A kinetic sorption approach accounting for the surface exclusion effects of previously deposited colloids of different sizes is also examined in this study. As a colloid travels through the fracture, the transport mechanisms (advection and diffusion) may eventually bring the particle close enough to the aperture surface to have the opportunity to establish a fracture wall contact resulting from local interaction forces between the colloid and the liquid-solid matrix interface. The probability of the particle being placed (sticking probability) per wall collision is calculated by the Boltzmann law [*Adamczyk et al*., 1991]

$$p = \exp\left[\frac{-\phi}{kT}\right] \tag{15}$$

where ϕ is the repulsive energy of interaction of the particle with the fracture surface ($\phi \simeq 10kT$) [*Adamczyk et al*., 1997]. The Boltzmann law assumes that if a particle comes into contact with a fracture wall it is either adsorbed with probability p or reflected. In this work a probabilistic sorption model is adopted to simulate the kinetic sorption of colloids [*Hinrichsen et al*., 1990]. In general, the probabilistic sorption model describing the time dependent concentration of the particles adsorbed onto the fracture surface is given by [*Adamczyk et al*., 1992a, *Chrysikopoulos and Abdel-Salam*, 1997]

$$\frac{\partial n^*}{\partial t} = r_f \frac{n}{b} - r_r n^* \tag{16}$$

where r_f and r_r are the forward and reverse colloid deposition rate constants, respectively. Particles accumulated on the surface of the fracture influence the transport and adsorption of other particles moving in their vicinity because of a geometric volume exclusion effect. Commonly, r_r is assumed to be negligible [*Bowen and Epstein*, 1979], whereas r_f can be expressed as

$$r_f = \tfrac{2}{3} U_{\max} p \kappa F(n^*) \tag{17}$$

where κ is the colloid deposition coefficient, and $F(n^*)$ is the DBF which takes into account the effect of previously deposited particles per unit fracture surface area on subsequent colloid deposition by specifying the portion of the fracture surface area that remains available for deposition.

Through the use of a random number generator the Boltzmann law (15) can incorporate the microscopic probability of attachment, p, into a macroscopic adsorption constant r_f. For example, if $\phi = 10kT$, then according to (15), $p = 4.54 \times 10^{-5}$. Thus roughly 2 particles per every 10^4 wall collisions will sorb onto a surface free of previously deposited colloids. The effect of deposited colloids can be taken into account through the use of a DBF, which ranges between one (for a fracture free of colloids) and zero (for a fracture surface completely covered by deposited colloids). When interstitial fluid and sorbent surface chemical conditions favor the attachment of stable colloid particles onto sorbent surfaces, colloid deposition is essentially irreversible and restricted to monolayer coverage [*Johnson et al*., 1996]. For the case of irreversible sorption the linear DBF (the area that remains available for a colloid to deposit onto the fracture wall) is given by [*Song and Elimelech*, 1994; *Chrysikopoulos and Abdel-Salam*, 1997]

$$F(n^*) = \frac{\varepsilon_{\max} - \varepsilon}{\varepsilon_{\max}} \tag{18}$$

where

$$\varepsilon(t, x) = A_p n^*(t, x) \tag{19}$$

$$\varepsilon_{\max} = \frac{1}{\beta} \tag{20}$$

and $A_p = \pi d_p^2/4$ is the cross-sectional area of a colloidal particle and β is a factor accounting for blocked area not directly covered by the colloid (excluded area) [*Rajagopalan*

and Chu, 1981]. Because of electrostatic repulsive forces, a sorbed colloid should effectively block more area than simply the space it physically occupies. For comparison, the following nonlinear DBF is also investigated in this study [*Adamczyk et al*., 1992b]:

$$F(n^*) = 1 - 2.184\left(\frac{\varepsilon}{\varepsilon_{\max}}\right) + 0.986\left(\frac{\varepsilon}{\varepsilon_{\max}}\right)^2 + 0.29\left(\frac{\varepsilon}{\varepsilon_{\max}}\right)^3 \tag{21}$$

The linear DBF is valid for spherical uncharged particles depositing onto a flat surface. At higher surface coverage ($\varepsilon \geq \varepsilon_{\max}/10$), (21) is a better estimate of the area blocked by the colloids and is valid for coverage up to $0.8\varepsilon_{\max}$ [*Adamczyk et al*., 1992a; *Chrysikopoulos and Abdel-Salam*, 1997].

2.4. Particle Tracking

Particle-tracking algorithms can provide stochastic solutions to linear partial differential equations like the advection-diffusion equation. Although the particle-tracking technique does not provide a direct numerical solution to a differential equation, it does not suffer from numerical dispersion as do the finite element and finite difference methods [*Thompson and Gelhar*, 1990]. It should be noted that particle tracking is the only method which can facilitate the use of variably sized colloids. Each particle is individually considered (i.e., stored in a memory location), and as such, it can retain its own unique characteristics including, for example, size and sorption status. The size of each colloid particle implicitly dictates its diffusion coefficient according to (5).

Particle-tracking techniques have been applied in numerous investigations of contaminant transport in porous and fractured media [*Ahlstrom et al*., 1977; *Smith and Schwartz*, 1980; *Kinzelbach and Uffink*, 1988; *Chrysikopoulos et al*., 1992; *Thompson et al*., 1996]. Particle tracking does not require an effective dispersion coefficient, such as (4) employed in the Taylor dispersion analysis, because the algorithm itself accounts for advective and diffusive transport in all directions (not just axial advection and longitudinal diffusion). The general particle-tracking transport equation consists of a nonstochastic or absolute term, the advection, and a stochastic term representing the random molecular diffusion [*Thompson*, 1993; *Kitanidis*, 1994]. In vector notation the particle-tracking equations are [*Thompson and Gelhar*, 1990]

$$\mathbf{X}^m = \mathbf{X}^{m-1} + \mathbf{A}(\mathbf{X}^{m-1})\Delta t + \mathbf{B}(\mathbf{X}^{m-1}) \cdot \mathbf{Z}\sqrt{\Delta t} \tag{22}$$

where m is the numerical step number, $\mathbf{X}^m$ is the three-dimensional position vector at time level $m\Delta t$, $\mathbf{A}(\mathbf{X}^{m-1})$ is the deterministic forcing vector (e.g., the velocity profile and/or deterministic velocities) evaluated at $\mathbf{X}^{m-1}$, $\mathbf{B}(\mathbf{X}^{m-1})$ is a deterministic scaling second-order tensor evaluated at $\mathbf{X}^{m-1}$ (e.g., a function of the molecular diffusion coefficient), and $\mathbf{Z}$ is a vector of three independent random numbers with zero mean and unit variance. The second-order tensor $\mathbf{B}(\mathbf{X}^{m-1})$ has nonzero terms, $\sqrt{2\mathscr{D}}$, along the diagonal [*Ahlstrom et al*., 1977]. In view of (22) the particle-tracking transport equations for the problem examined in this work without deterministic velocities or gravitational terms can be written as

$$x^m = x^{m-1} + U_{\max}\left[1 - 4\left(\frac{y^{m-1}}{b}\right)^2\right]\Delta t + Z_1\sqrt{2\mathscr{D}\Delta t} \tag{23}$$

$$y^m = y^{m-1} + Z_2\sqrt{2\mathscr{D}\Delta t} \tag{24}$$

Because it is simplest to work with nondimensional variables, (23) and (24) are nondimensionalized as follows:

$$\hat{x}^m = \hat{x}^{m-1} + \hat{u}[1 - 4(\hat{y}^{m-1})^2] + Z_1\sqrt{2\hat{D}} \tag{25}$$

$$\hat{y}^m = \hat{y}^{m-1} + Z_2\sqrt{2\hat{D}} \tag{26}$$

where

$$\hat{x} = \frac{x}{b} \tag{27}$$

$$\hat{y} = \frac{y}{b} \tag{28}$$

$$\hat{u} = \frac{U_{\max}\Delta t}{b} \tag{29}$$

$$\hat{D} = \frac{\mathscr{D}\Delta t}{b^2} \tag{30}$$

2.5. Numerical Procedures

2.5.1. Transport. The particle-tracking model developed in this work assumes that every individual particle undergoes an incremental movement during each time step. Initially, all particles are randomly distributed along the y axis at $x = 0$; they are contained within the fracture without any particle-wall overlap. Particle-particle interactions are not accounted for. A large number of particles, of the order of 150,000, is used in an effort to reduce random noise [*Valocchi and Quinodoz*, 1989]. Although by increasing the number of particles more computation time is required, a large number of particles leads to smoother results by averaging out the effect of individual particles. As in any averaging process, the larger the sample size, the less the contribution of a single component and the more smooth and regular the results. At each time level a new particle position is determined from (25) and (26). The time step is specified so that the maximum distance a particle can travel by diffusion during a time step Δt is less than the fracture aperture b. Consequently, a particle reflected from one side of the aperture may not end up in the rock matrix at the other side. For the case where the solid matrix is impermeable (zero porosity) all particles are reflected from the wall as in a mirror image without loss of energy. That is, the final x coordinate position remains unchanged, whereas the final y coordinate is set a distance away from the wall equal to the distance that the particle would have obtained if it had penetrated the rock matrix.

2.5.2. Matrix diffusion. For permeable solid matrices each time a particle reaches a fracture surface, its probability of penetrating the matrix is proportional to the matrix porosity. For example, when a colloid contacts a solid matrix with porosity 0.01, it has a 1% chance of encountering a void space of that solid matrix. A random number between 0 and 1 (uniformly distributed) is generated every time a particle encounters a wall, and if this number is less than the porosity, the colloid is assumed to enter the matrix. It is assumed that a particle entering a solid matrix continues to migrate within the pore as it was in the fracture only for the remaining portion of the time step because when a particle enters a pore, it still experiences an effective porosity of 1.0, and its diffusivity is not altered from that in the fracture. Although the probability of penetrating the matrix is independent of particle size, once in the matrix, particle diameter affects how a particle is trans-

ported according to its diffusion coefficient (which is also present in both (7) and (8)). As the rock matrix interferes with colloid diffusion, the diffusion coefficient is also proportional to the solid matrix porosity (i.e., the value of the particle diffusion coefficient within a solid matrix with porosity 0.1 is assumed to be $\mathcal{D}/10$) [*Buckley and Loyalka*, 1993]. Although wall effects on diffusion and velocity are well known, no modification to diffusivity or particle velocity in the fracture near the walls is performed as the time step used in this analysis is too large to account for such corrections.

In order to incorporate (7) and (8) into the particle-tracking equation a transition zone just inside the solid matrix was defined. The gradients of diffusivity and porosity were assumed to vary linearly over this zone which was chosen to be one half of the fracture width. Thus the differences between matrix and fracture diffusivities and log porosities were calculated and then divided by the transition zone thickness to determine gradients in the transition zone. Thus (7) and (8) are expressed as

$$U_{\mathcal{D}} = \frac{2\mathcal{D}(\theta - 1)}{b} \tag{31}$$

$$U_{\theta} = \frac{2\mathcal{D} \ln \theta}{b} \tag{32}$$

If a particle is within the matrix and less than a distance of $b/2$ from the fracture wall, $U_{\mathcal{D}}$ and U_{θ} are multiplied by Δt and added to the particle-tracking equation in the y direction

$$y^m = y^{m-1} + Z_2\sqrt{2\mathcal{D}\Delta t} + U_{\mathcal{D}}\Delta t + U_{\theta}\Delta t \tag{33}$$

Ultimately, a particle is allowed to diffuse back into the fracture, and the inclusion of $U_{\mathcal{D}}$ and U_{θ} serves to avoid the uncharacteristic buildup of particles in stagnation or low-porosity zones. Any colloid size distribution (e.g., lognormal, Gaussian, or uniform) could be used in this particle-tracking transport model.

2.5.3. Deposition. For the case of perfect sink attachment (employing the Smulochowski-Levich approximation to determine K_d) the fracture walls and channel aperture are discretized into length elements. Each element comprises a segment of the fracture walls, both top and bottom, along the x direction. A triply nested sorting algorithm was developed to arrange the colloids first according to x location, then size, and finally, y location. At the beginning of every time step the number of colloids contained within each length element of the fracture is calculated. Within each length element the colloids are subdivided into 10 equally sized "bins" according to diameter. The size of each bin is set equal to the difference between the largest and smallest colloid diameters of the particles present within each element divided by 10. Subsequently, the flux of particles onto the surface within each element of each bin is determined according to (13). The flux J multiplied by the time step Δt (rounded to the nearest integer) indicates how many particles sorb onto each length element of the fracture from each bin during each time step. The particles nearest the wall (greatest y location) are assumed to attach. An exact particle balance is maintained by tagging each adsorbed particle with an integer associated with its length element. That is, the number of attached particles is plotted against their associated length element. This process is repeated for each time step. Desorption is based on the number of sorbed particles, n^*. Because colloids are assumed to sorb irreversibly, the desorption rate is assigned a small enough value to be considered as negligible.

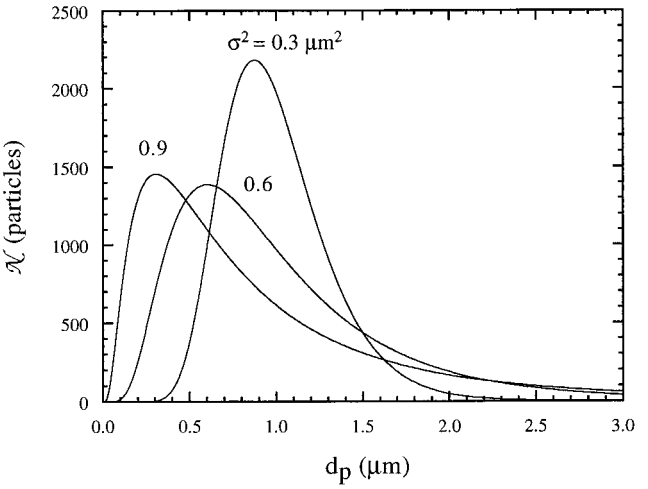

Figure 3. Illustration of three lognormal distributions of colloid diameters with $\mu = 1 \times 10^{-6}$m and $\sigma^2 = 0.3, 0.6, 0.9\ \mu m^2$.

When particles undergo kinetic sorption, the fracture wall is also discretized into length elements. Each time a particle comes in contact with the wall, its chance of sorbing is based on the number of previously sorbed colloids, n^*, and the particle-wall repulsive energy ϕ. After each time step the number of sorbed colloids in each element of fracture wall is determined in order to recalculate the sorption probability of a colloid onto that element according to relationship (18) or (21). As the number of sorbed colloids increases, the probability of future sorption decreases. The fracture surface area that remains available for deposition depends on the size of the sorbed colloids.

3. Simulations and Discussion

3.1. Model Parameters

Particle-tracking simulations of 150,000 particles were conducted following the previously described procedures. The diameter of each particle, d_p, was assigned a discrete quantized value accurate to one hundredth of a micrometer. The three lognormal colloid size distributions with mean $\mu = 1 \times 10^{-6}$m and variances of $\sigma^2 = 0.3$, 0.6, and 0.9 μm^2 used in this study are shown in Figure 3. Unless otherwise specified, the simulations presented in this work are obtained with $U_{\max} = 1 \times 10^{-6}$m s^{-1} and $b = 1 \times 10^{-4}$m. Table 1 summarizes all model parameters.

3.2. Comparison With an Analytical Solution

In order to check the accuracy of the particle-tracking modeling technique described in this work a distribution curve generated with the analytical solution for the ideal case of monodisperse particle transport in a parallel plate system, (6), is compared to appropriate particle-tracking results. It is worth discussing how the particle number concentration is determined and how the results are presented. The particle-tracking simulation only returns the two-dimensional x and y coordinates of each colloid, yet from this data a concentration is to be determined. First, the maximum and minimum x coordinates of all particles are found in order to calculate the range of values. This range is then divided into equal length subsections or bins and the number of particles that fall into each bin is

Table 1. Model Parameters for Simulations

Parameter	Value	Reference
b	1×10^{-4} m	*Reimus* [1995]
r_r	~ 0 s^{-1}	
U_{max}	1×10^{-6} m s^{-1}	*Reimus* [1995]
β	15	*Chrysikopoulos and Abdel-Salam* [1997]
Δt	150 s	
θ	0 − 0.1	*Buckley and Loyalka* [1994]
μ	1×10^{-6} m	*Ledin et al.* [1994]
σ^2	0.3, 0.6, 0.9 μm^2	
ϕ	4.04×10^{-19} J per colloid	*Adamczyk et al.* [1997]

determined (as would be done with a histogram). Since the length of the bin is known, as is the aperture width, the number of colloids within this area can be determined and presented as an areal concentration (particles per cm^{-2}). Similarly, for a three-dimensional fracture the corresponding volume concentrations should be expressed in (particles per cm^3). Figure 4 shows an excellent agreement between the analytical solution and the particle-tracking simulation. The introduction of random noise, ubiquitous in random walk methods, is evident as the particle-tracking distribution is not completely smooth [*Uffink*, 1988]. It should be noted that the Taylor analysis makes the simplifying assumption that the effect of longitudinal diffusion is small enough to be neglected. This assumption is not employed by the particle-tracking model.

3.3. Effects on Spreading

Model simulations of variably sized colloid transport in a fracture are compared to the case of a monodisperse colloid suspension. Figure 5 shows how three lognormally distributed colloid plumes (σ^2 = 0.3, 0.6, and 0.9 μm^2) compare to a monodisperse colloid suspension at a distance of 12 m downstream from the fracture inlet (injection point). The larger the range of colloid sizes (large σ^2), the greater the observed spreading. Thus, by adding an extra degree of heterogeneity to the system (i.e., the variable colloid size distribution) the spreading of the colloid plume was enhanced. This is analogous to the case of virus transport in porous media (viruses are considered as colloid particles) where increased spreading is predicted with increased sorption variations caused by fluctuating external conditions [*Chrysikopoulos and Sim*, 1996].

To examine the effect of colloid size on spreading, at the end of 5000 hours of simulation time, each of the three lognormal diameter size distributions was divided into three groups with equal numbers of particles (50,000 particles). Histograms of colloid diameter for each of the three groups and each standard deviation examined are presented in Figure 6. The first group is indicated in Figure 6 with open circles and represents the slowest colloids, i.e., the colloids located nearest to the fracture inlet at the end of the simulation. The second group is indicated by the solid circles and represents the portion of the particles which are located in the middle of the cloud. The third group is indicated by squares and represents the particles that have traveled farthest within the fracture. Although the distribution of each group retains a lognormal shape, it is clear that a separation of colloids based on size is occurring. The larger colloids travel farther and faster than the smaller colloids. Several researchers [e.g., *Grindrod*, 1993; *Ryan and Elimelech*, 1996] have hypothesized that a colloid's finite dimen-

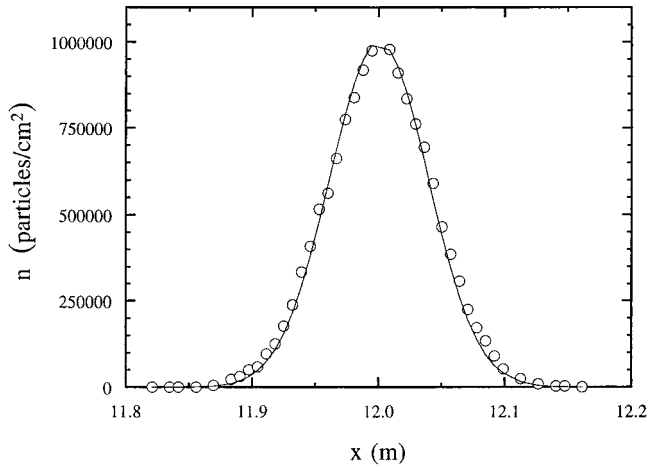

Figure 4. Comparison of an analytical solution based on Taylor's assumptions (solid line) and the particle-tracking simulation for a monodisperse ($d_p = 1 \times 10^{-6}$m) colloid suspension (circles) at 208 days after the introduction of the colloid pulse in a fracture with uniform aperture. Because of the two-dimensional nature of the fracture considered, areal colloid concentrations are presented.

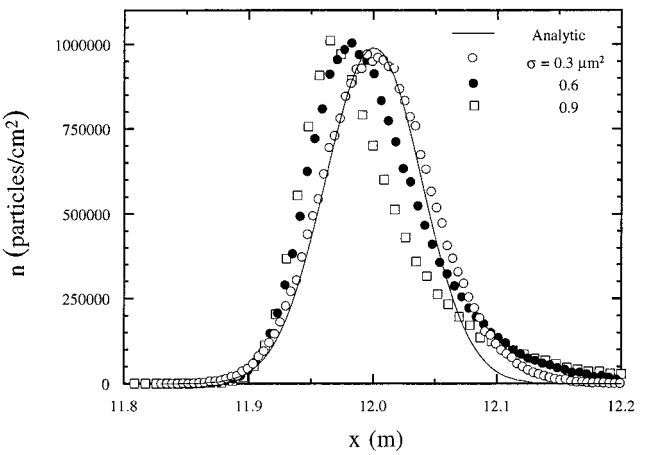

Figure 5. Comparison of the analytical solution (solid line) and the particle-tracking simulations for colloid plumes having lognormal diameter distributions with $\mu = 1 \times 10^{-6}$m and σ^2 = 0.3 (open circles), σ^2 = 0.6 (solid circles), and σ^2 = 0.9 μm^2 (squares). Because of the two-dimensional nature of the fracture considered, areal colloid concentrations are presented (here t = 208 days).

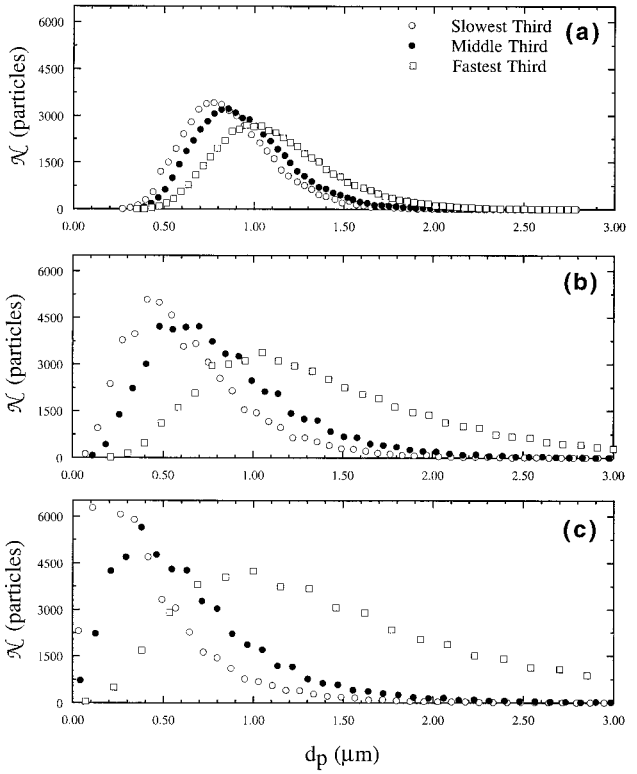

Figure 6. Number of colloids with a given diameter for plumes of colloids with lognormal diameter distributions with $\mu = 1 \times 10^{-6}$m and (a) $\sigma^2 = 0.3$, (b) $\sigma^2 = 0.6$ and (c) $\sigma^2 = 0.9$ μm^2 (here $t = 208$ days). The colloids have been divided into thirds on the basis of their distances from injection. The squares represent the fastest third; the solid circles represent the middle third; and the open circles represent the slowest third (closest to the inlet).

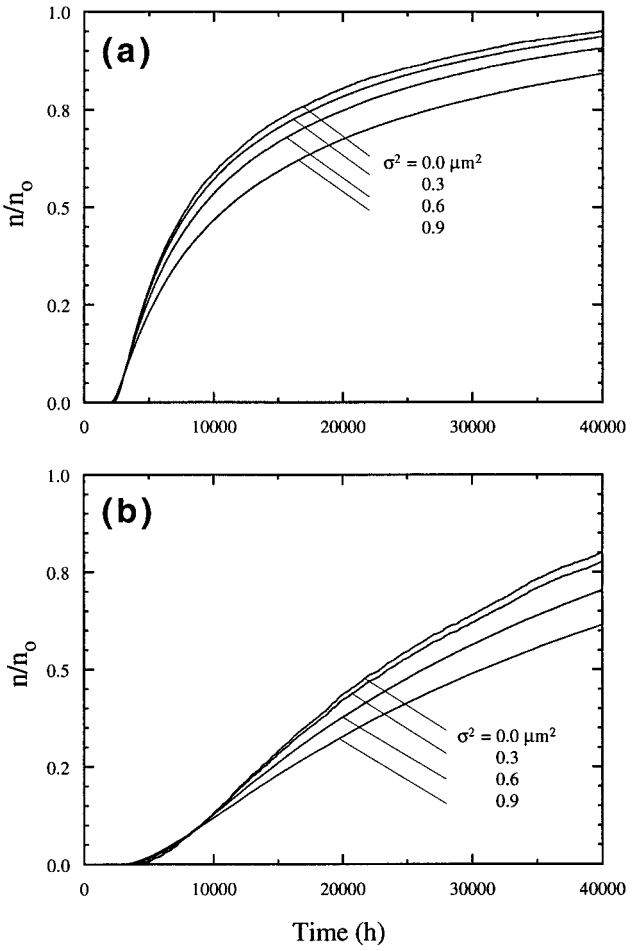

Figure 7. Normalized breakthrough curves for plumes of colloids having different lognormal distributions of particle diameters in a fracture with uniform aperture and (a) 1% and (b) 10% solid matrix porosity (here $x = 5$ m).

sions prohibit it from contacting the slowest moving fluid near the fracture boundaries and thus force it to be advected at a velocity slightly faster than the average fluid velocity. Clearly, Figure 6 shows that on average the largest colloid particles are advected faster than the smaller particles.

3.4. Effects of Matrix Diffusion

The effect of matrix diffusion on colloid breakthrough curves at a distance of 5 m from the fracture inlet for the monodisperse and the three different lognormal colloid size distributions is illustrated in Figure 7. Clearly, different colloid size distributions lead to distinct breakthrough patterns. The higher the standard deviation of the colloid size distribution, the more pronounced is the retardation of the colloid plume. In particular, the plume with the largest colloid size standard deviation contains the largest number of small colloids. These smaller particles are transported the slowest not only because they can sample the slowest moving portion of the parabolic velocity profile (nearest to the wall) but because smaller colloids preferentially diffuse into the rock matrix.

The probability for diffusion into the fracture wall is dependent on the matrix porosity alone. However, the number of times that a colloid contacts the wall is a function of its diffusion coefficient. Because of their large diffusion coefficient (large diffusive travel distance per time step), smaller particles are more likely to come into contact with the fracture wall. Each time a particle contacts the wall there is a certain probability that it will diffuse into it. The more times a particle encounters a wall, the higher the overall probability that it will diffuse into the solid matrix. The deterministic velocities added to the particle-tracking equations serve to account for back diffusion into the fracture once the bulk of the colloid cloud has passed. Although some particles are effectively lost from the system by diffusing well into the rock matrix (past the transition zone), many are pushed back into the fracture by the concentration gradient remaining when few colloids are left in the fracture. Smaller colloids are more likely to diffuse into (and be transported out of) the matrix. This effectively increases the residence time of small colloids and retards the breakthrough of large variance colloid plumes with many small colloid constituents.

3.5. Colloid Deposition

3.5.1. Perfect sink. Figure 8 presents the sorbed colloid concentrations n^* after ~208 days of simulation time for each of the three colloid suspensions considered in this study ($\sigma^2 =$ 0.3, 0.6, and 0.9 μm^2). The results for the two-dimensional fracture considered here are presented in units of particles per cm; however, for a fully three-dimensional fracture the corre-

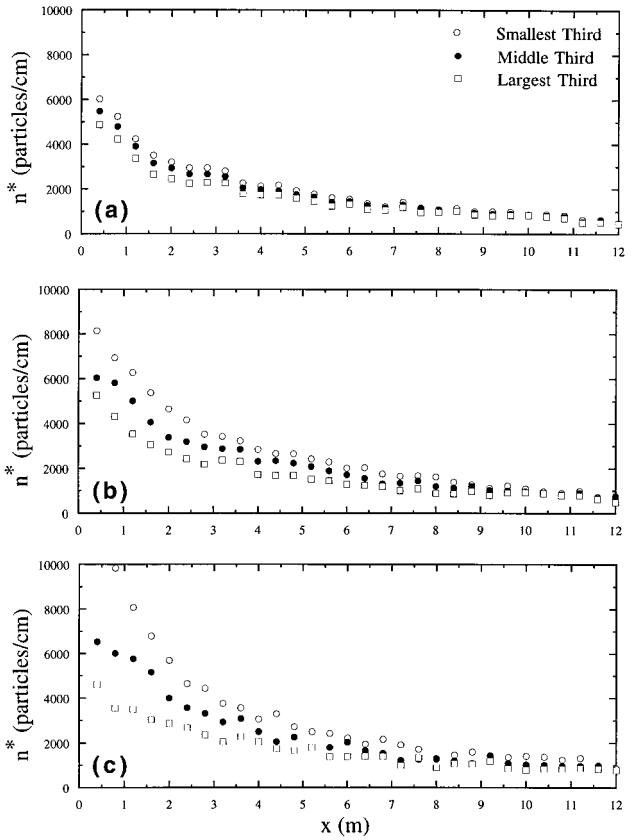

Figure 8. Sorbed colloid concentrations under perfect sink conditions as a function of fracture length for colloid plumes having lognormal diameter distribution with $\mu = 1 \times 10^{-6}$m and (a) $\sigma^2 = 0.3$, (b) $\sigma^2 = 0.6$, and (c) $\sigma^2 = 0.9$ μm^2. The colloids have been divided into thirds on the basis of their diameter size. The open circles represent the smallest third; the solid circles represent the middle third; and the squares represent the largest third (here $t = 208$ days).

sponding units are particles per cm^2. The colloids are divided into three groups of 50,000 particles according to size. It is evident from Figure 8 that the smallest colloids show the highest sorbed concentration. Therefore preferential sorption of small colloids occurs. Also, the number of deposited colloids as a function of fracture length follows an $x^{-1/3}$ dependence as indicated by the flux relationship (13). The concentration of colloids in the liquid phase decreases as more colloids sorb onto the fracture surface.

3.5.2. Kinetic. Figure 9 shows snapshots of the sorbed colloid concentrations n^* under linear kinetic sorption conditions for each of the three lognormal colloid distributions considered in this study ($\sigma^2 = 0.3$, 0.6, and 0.9 μm^2). Because of their larger diffusion coefficients, preferential sorption of small colloids over larger colloids is expected as they will contact the wall more frequently than larger colloids. This is clearly illustrated in Figure 9 where the colloid suspension with the largest variance, $\sigma^2 = 0.9$ μm^2, (and thus the largest number of small colloids) exhibits the greatest sorption near the entrance to the fracture. Figure 10 presents the colloids divided into three groups of 50,000 particles arranged according to diameter in order to reveal any possible trend of preferential sorption. The group with the largest colloids exhibits the least sorption, while the group with the smallest colloids yields the highest concentration of colloids sorbed. As smallest particles have the largest Brownian diffusion rate, they come into contact with the fracture wall more often than the larger particles and, consequently, have a higher sorption rate as is illustrated in Figure 10.

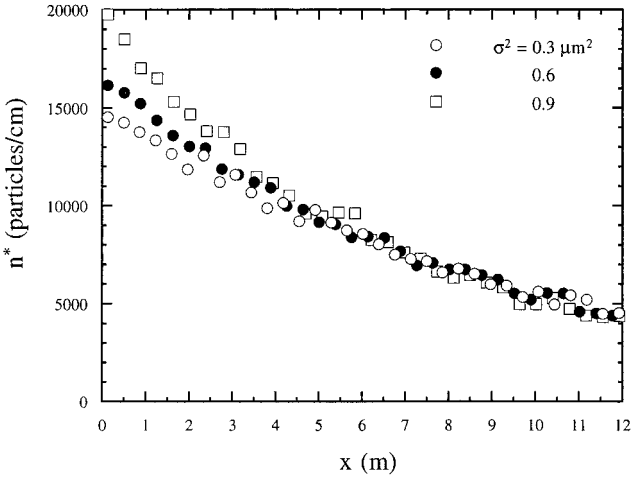

Figure 9. Overall sorbed colloid concentrations under linear kinetic sorption conditions as a function of fracture length for colloid plumes with different colloid diameter distributions and $\mu = 1 \times 10^{-6}$m (here $t = 208$ days and $\phi = 10kT$). Because of the two-dimensional nature of the fracture considered, sorbed colloid concentrations per unit length are presented.

Figure 11 compares the effect of linear and nonlinear DBFs on sorbed colloid concentrations. The results are comparable for all three distributions with the nonlinear DBF leading to slightly lower sorbed colloid concentrations than the linear case. In view of (21) this is an expected result because for a small number of sorbed particles, the nonlinear DBF behaves like the linear DBF. Only for a relatively large number ($\varepsilon \geq \varepsilon_{max}/10$) of sorbed particles per length element does the nonlinear case substantially deviate from the linear DBF in the form of a reduced sorption probability.

3.6. Effect of Fracture Aperture

In order to examine the effect of fracture aperture on colloid deposition onto fracture walls, particle-tracking simulations were conducted for fractures with varying aperture widths while keeping all other transport parameters constant. A monodisperse colloid suspension is employed. Furthermore, it was assumed that colloids follow a linear kinetic sorption relationship. The results presented in Figure 12 indicate that the sorbed colloid concentration is inversely proportional to the aperture width. The number of kinetically sorbed colloids from a monodisperse suspension decreases with increasing fracture aperture. As the aperture is increased, it is less likely that a colloid will contact the wall. This is in agreement with the proposed expression for the mass flux of colloids onto fracture surfaces presented by *Abdel-Salam and Chrysikopoulos* [1994, 1995a, b].

4. Summary and Conclusions

In this study the transport of polydisperse colloid plumes in a fully saturated fracture with a uniform aperture was modeled

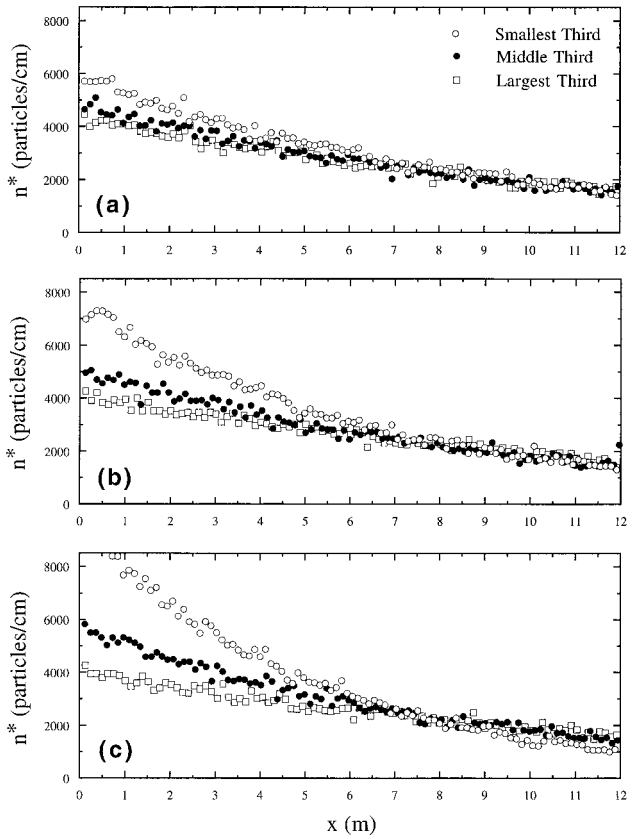

Figure 10. Sorbed colloid concentrations under linear kinetic sorption conditions as a function of fracture length for colloid plumes having lognormal diameter distribution with $\mu = 1 \times 10^{-6}$m and (a) $\sigma^2 = 0.3$, (b) $\sigma^2 = 0.6$, and (c) $\sigma^2 = 0.9$ μm^2. The colloids have been divided into thirds on the basis of their diameter size (here $t = 208$ days and $\phi = 10kT$).

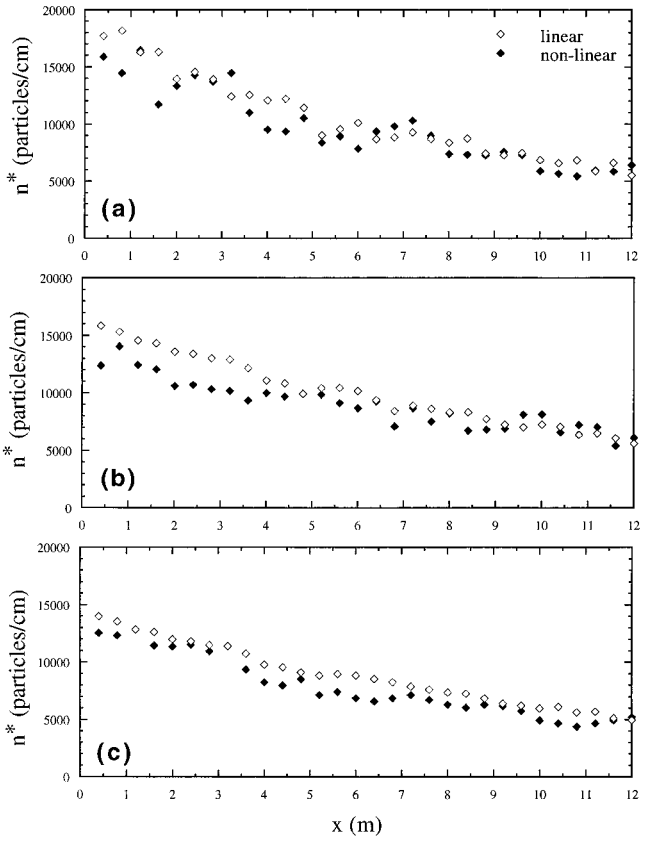

Figure 11. Effect of linear (open diamonds) and nonlinear (solid diamonds) kinetic dynamic blocking functions (DBFs) on sorbed colloid concentrations along the fracture for colloid plumes having lognormal diameter distributions with $\mu = 1 \times 10^{-6}$m and (a) $\sigma^2 = 0.3$, (b) $\sigma^2 = 0.6$, and (c) $\sigma^2 = 0.9$ μm^2.

by particle-tracking techniques. Both the effects of matrix diffusion and surface sorption were investigated. Simulation results show that polydisperse colloid suspensions exhibit different transport characteristics than monodisperse suspensions. The observed spreading of polydisperse colloid plumes is proportional to the variance of the colloid diameter distribution. Small colloids have a large molecular diffusion coefficient, while large colloids have a large Taylor dispersion coefficient. Therefore large colloids have an earlier first arrival time because of greater dispersion leading to an increased spreading of the plume. Breakthrough curves of polydisperse colloid suspensions in fractures with different matrix porosities indicate that a plume with larger variance in colloid diameter becomes progressively more retarded owing to the increased number of small colloids which are more often trapped in the solid matrix. It can be concluded that the increased retardation for colloid plumes with higher variance of the colloid diameter distribution is due to both the slower average velocity of the smallest particles and their preferential diffusion into the solid matrix. Colloid sorption is shown to be affected by particle size with the smallest particles preferentially sorbing onto the fracture walls. The linear and nonlinear kinetic sorption models examined in this work may lead to substantially different sorbed colloid distributions when the fracture surface area covered by the sorbed colloids is relatively large. Furthermore, it was demonstrated that particle sorption is inversely proportional to the fracture aperture. This investigation lays the groundwork for future studies of more realistic situations including transport in variable aperture fractures and in fracture networks.

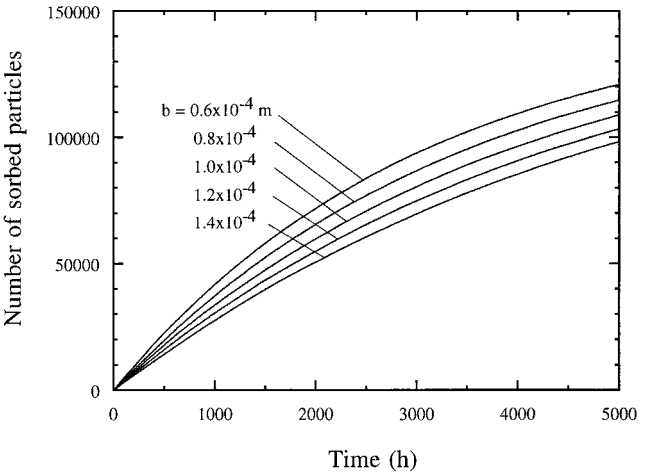

Figure 12. Total number of sorbed colloids from a monodisperse suspension ($d_p = 1 \times 10^{-6}$m) as a function of time for several different fracture aperture widths.

Notation

A_p projected (cross-sectional) area of a colloidal particle: $\pi d_p^2/4$ (L^2).
$\mathbf{A}$ deterministic forcing vector (Lt^{-1}).
b fracture aperture width (L).
$\mathbf{B}$ deterministic scaling tensor ($Lt^{-1/2}$).
d_p diameter of a colloidal particle (L).
D^* Taylor dispersion coefficient (L^2t^{-1}).
$\hat{D}$ non-dimensional diffusion coefficient.
$\mathcal{D}$ molecular diffusion coefficient in the fracture (L^2t^{-1}).
$F(n^*)$ dynamic blocking function.
J particle number flux at the fracture surface ($M^{-2}t^{-1}$).
k Boltzmann's constant ($ML^2t^{-2}T^{-1}$).
K_d partition coefficient for colloid deposition onto fracture surfaces (L).
m time step number.
n number concentration of colloids per unit volume of liquid (L^{-3}).
n_o initial number concentration of colloids per unit volume of liquid (L^{-3}).
n^* colloid number concentration deposited per unit fracture surface area (L^{-2}).
$\mathbf{n}$ unit normal vector (L).
$\mathcal{N}(d_p)$ number of colloids of a given diameter, d_p.
$\mathcal{N}_o$ total number of colloids introduced into the fracture.
p probability of sorption from Boltzmann law.
Pe Peclet number.
r_f forward colloid deposition rate coefficient (L^2t^{-1}).
r_r reverse colloid deposition rate coefficient (t^{-1}).
Sh Sherwood number.
t time (t).
T absolute temperature of the solvent (T).
$\hat{u}$ nondimensional velocity.
$U_{\mathcal{D}}$ deterministic velocity due to diffusivity gradient (Lt^{-1}).
$U_{\max}$ maximum velocity along the centerline in the x direction (Lt^{-1}).
U_θ deterministic velocity due to porosity gradient (Lt^{-1}).
U_x fracture flow velocity in the x direction (Lt^{-1}).
x coordinate along the fracture length (L).
x' distance from the center of mass of the colloid plume (L).
$\hat{x}$ nondimensional coordinate along the fracture length.
$\mathbf{X}$ three-dimensional position vector (L).
y coordinate along the fracture width (L).
$\hat{y}$ nondimensional coordinate along the fracture width.
Z_1, Z_2 randomly generated numbers with zero mean and unit variance.
$\mathbf{Z}$ randomly generated three-dimensional vector with zero mean and unit variance.
β scaling factor for fracture surface area blocked by a deposited colloid particle.
ε fraction of a fracture surface area covered (blocked) by deposited colloids.
$\varepsilon_{\max}$ fraction of a fracture surface area covered (blocked) by deposited colloids when n^* reaches its maximum.
ζ^2 variance of the log-colloid diameter distribution.
η dynamic viscosity of the interstitial fluid ($ML^{-1}t^{-1}$).
θ matrix porosity.
κ colloid deposition coefficient (L).
λ mean of the log-colloid diameter.
μ mean of the colloid diameter (L).
σ^2 variance of the colloid diameter distribution (L^2).
ϕ particle wall repulsive energy (ML^2t^{-2}).

Acknowledgments. This work was supported in part by the University of California, Irvine, through an allocation of computer resources on the SPP2000. The writers thank P. Reimus for his helpful suggestions.

References

Abdel-Salam, A., and C. V. Chrysikopoulos, Analytical solutions for one-dimensional colloid transport in saturated fractures, *Adv. Water Resour.*, *17*, 283–296, 1994.

Abdel-Salam, A., and C. V. Chrysikopoulos, Modeling of colloid and colloid-facilitated contaminant transport in a two-dimensional fracture with spatially variable aperture, *Transp. Porous Media*, *20*, 197–221, 1995a.

Abdel-Salam, A., and C. V. Chrysikopoulos, Analysis of a model for contaminant transport in fractured media in the presence of colloids, *J. Hydrol.*, *165*, 261–281, 1995b.

Adamczyk, Z., and T. G. M. van de Ven, Deposition of particles under external forces in laminar flow through parallel-plate and cylindrical channels, *J. Colloid Interface Sci.*, *80*, 340–356, 1980.

Adamczyk, Z., T. Dabros, J. Czarnecki, and T. G. M. van de Ven, Kinetics of particle accumulation at collector surfaces, I, Approximate analytical solutions, *Adv. Colloid Interface Sci.*, *19*, 183–252, 1983.

Adamczyk, Z., B. Siwek, and M. Zembala, Kinetics of localized adsorption of particles on homogeneous surfaces, *J. Colloid Interface Sci.*, *151*, 351–367, 1991.

Adamczyk, Z., B. Siwek, and M. Zembala, Reversible and irreversible adsorption of particles on homogeneous surfaces, *Colloids Surf.*, *62*, 119–130, 1992a.

Adamczyk, Z., B. Siwek, M. Zembala, and P. Weronski, Kinetics of localized adsorption of colloid particles, *Langmuir*, *8*, 2605–2610, 1992b.

Adamczyk, Z., B. Siwek, M. Zembala, and P. Weronski, Influence of polydispersity on random sequential adsorption of spherical particles, *J. Colloid Interface Sci.*, *185*, 236–244, 1997.

Ahlstrom, S. W., H. P. Foote, R. C. Arnett, C. R. Cole, and R. J. Serne, *Multicomponent Mass Transport Model: Theory and Numerical Implementation* (*Discrete-Parcel-Random-Walk Version*), Atlantic Richfield Hanford, Richland, Washington, 1977.

Ang, A. H.-S., and W. H. Tang, *Probability Concepts in Engineering Planning and Design*, John Wiley, New York, 1975.

Berkowitz, B., and H. Scher, On characterization of anomolous dispersion in porous and fractured media, *Water. Resour. Res.*, *31*, 1461–1466, 1995.

Berkowitz, B., and J. Zhou, Reactive solute transport in a single fracture, *Water Resour. Res.*, *32*, 901–913, 1996.

Bird, R. B., W. E. Stewart, and E. N. Lightfoot, *Transport Phenomena*, John Wiley, New York, 1960.

Bowen, D. D., and N. Epstein, Fine particle deposition in smooth parallel plate channels, *J. Colloid Interface Sci.*, *72*, 81–97, 1979.

Buckley, R. I., and S. K. Loyalka, Radionuclide migration in fractured media: Numerical studies of advection/diffusion in a fracture and diffusion in the surrounding rock matrix, *Ann. Nucl. Energy*, *20*, 701–718, 1993.

Buckley, R. I., and S. K. Loyalka, Numerical studies of solute transport in a fracture surrounded by rock matrix: Effect of lateral diffusion and chemical reactions on the overall dispersion, *Ann. Nucl. Energy*, *21*, 461–494, 1994.

Chrysikopoulos, C. V., and A. Abdel-Salam, Modeling colloid transport and dispersion in saturated fractures, *Colloids Surfaces A*, *121*, 189–202, 1997.

Chrysikopoulos, C. V., and Y. Sim, One-dimensional virus transport in homogeneous porous media with time dependent distribution coefficient, *J. Hydrol*., *185*, 199–219, 1996.

Chrysikopoulos, C. V., P. K. Kitanidis, and P. V. Roberts, Generalized Taylor-Aris moment analysis of the transport of sorbing solutes through porous media with spatially-periodic retardation factor, *Transp. Porous Media*, *7*, 163–185, 1992.

Chung, J. Y., and K. J. Lee, Analysis of colloid transport and colloidal size effect using filtration theory, *Ann. Nucl. Energy*, *19*, 145–153, 1992.

Edwards, D. A., M. Shapiro, H. Brenner, and M. Shapira, Dispersion of inert solutes in spatially periodic two-dimensional model porous media, *Transp. Porous Media*, *6*, 337–358, 1991.

Elimelech, M., J. Gregory, X. Jia, and R. Williams, *Particle Deposition and Aggregation: Measurement, Modeling and Simulation, Butterworth-Heinemann*, Newton, Mass., 1995.

Fox, R. W., and A. T. McDonald, *Introduction to Fluid Mechanics*, 4th ed., John Wiley, New York, 1992.

Gelhar, L., *Stochastic Subsurface Hydrology*, Prentice-Hall, Englewood Cliffs, N. J., 1993.

Grindrod, P., The impact of colloids on the migration and dispersal of radionuclides within fractured rock, *J. Contam. Hydrol*., *13*, 167–181, 1993.

Grisak, G. E., and J. F. Pickens, An analytical solution for solute transport through fractured media with matrix diffusion, *J. Hydrol*., *52*, 47–57, 1981.

Hinrichsen, E. L., J. Feder, and T. Jossang, Random packing of disks in two dimensions, *Phys. Rev. A*, *41*, 4199–4209, 1990.

Ibaraki, M., and E. A. Sudicky, Colloid-facilitated contaminant transport in discretely fractured porous media, 1, Numerical formulation and sensitivity analysis, *Water Resour. Res*., *31*, 2945–2960, 1995.

Johns, R. A., and P. V. Roberts, A solute transport model for channelized flow in a fracture, *Water Resour. Res*., *27*, 1797–1808, 1991.

Johnson, R., S. Ning, and M. Elimelech, Colloid transport in geochemically heterogeneous porous media: Modeling and measurements, *Environ. Sci. Technol*., *30*, 3284–3293, 1996.

Keller, A. A., P. V. Roberts, and P. K. Kitanidis, Prediction of single phase transport parameters in a variable aperture fracture, *Geophys. Res. Lett*., *22*, 1425–1428, 1995.

Kessler, J. H., and J. R. Hunt, Dissolved and colloidal transport in a partially clogged fracture, *Water Resour. Res*., *30*, 1195–1206, 1994.

Kinzelbach, W., and G. J. M. Uffink, The random walk method in pollutant transport simulation, in *Groundwater Flow and Quality Modeling*, edited by E. Custodio et al., pp. 227–245, D. Reidel, Norwell, Mass., 1988.

Kitanidis, P. K., Particle-tracking equations for the solution of the advection-dispersion equation with variable coefficients, *Water Resour. Res*., *30*, 3225–3227, 1994.

Ledin, A., S. Karlsson, A. Duker, and B. Allard, Measurements in situ of concentration and size distribution of colloidal matter in deep groundwater by photon correlation spectroscopy, *Water Res*., *28*, 1539–1545, 1994.

Neretnieks, I., T. Eriksen, and P. Tahtimen, Tracer movement in a single fissure in granitic rock: Some experimental results and their interpretation, *Water Resour. Res*., *18*, 849–858, 1982.

Payatakes, A. C., C. Tien, and R. M. Turian, Trajectory calculation of particle deposition in deep bed filtration, 1, Model formulation, *AIChE J*., *20*, 889–900, 1974.

Rajagopalan, R., and R. Q. Chu, Dynamics of adsorption of colloidal particles in packed beds, *J. Colloid Interface Sci*., *86*, 299–317, 1981.

Reimus, P. W., The use of synthetic colloids in tracer transport experiments in saturated rock fracture, *Rep. LA-13004-T*, Los Alamos National Laboratory, Los Alamos, N. M., 1995.

Ryan, J. N., and M. Elimelech, Colloid mobilization and transport in groundwater, *Colloids Surf. A*, *107*, 1–56, 1996.

Schaaf, H., and J. Talbot, Surface exclusion effects in adsorption processes, *J. Chem. Phys*., *91*, 4401–4409, 1989.

Smith, L., and F. W. Schwartz, Mass transport, 1, A stochastic analysis of macrodispersion, *Water Resour. Res*., *16*, 303–313, 1980.

Smith, P. A., and C. Degueldre, Colloid-facilitated transport of radionuclides through fractured media, *J. Contam. Hydrol*., *13*, 143–166, 1993.

Song, L., and M. Elimelech, Transient deposition of colloidal particles in heterogeneous porous media, *J. Colloid Interface Sci*., *167*, 301–313, 1994.

Statens Karnkraftinspektion, (SKI) (Swedish Nuclear Power Inspectorate, Project-90, *Tech. Rep*. *91(23)*, Stockholm, Sweden, 1991.

Taylor, G. I., Dispersion of soluble matter in solvent flowing slowly through a tube, *Proc. R. Soc. London*, *Ser. A*, *219*, 186–194, 1953.

Thompson, A. F. B., Numerical simulation of chemical migration in physically and chemically heterogeneous porous media, *Water Resour. Res*., *29*, 3709–3726, 1993.

Thompson, A. F. B., and L. W. Gelhar, Numerical simulation of solute transport in three-dimensional, randomly heterogeneous porous media, *Water Resour. Res*., *26*, 2541–2562, 1990.

Thompson, A. F. B., A. L. Schafer, and R. W. Smith, Impact of physical and chemical heterogeneity on cocontaminant transport in a sandy porous medium, *Water Resour. Res*., *32*, 801–818, 1996.

Uffink, G. J. M., Modeling of solute transport with the random walk method, *Groundwater Flow and Quality Modeling*, pp. 247–265, D. Reidel, Norwell, Mass., 1988.

Valocchi, A. J., and H. A. M. Quinodoz, Application of the random walk method to simulate the transport of kinetically adsorbing solutes, *Groundwater Contamination: Proceedings of the Symposium Held During the Third IAHS Scientific Assembly at Baltimore*, *May 1989*, edited by L. M. Abriola, *IAHS Publ*., *185*, 35–42, 1989.

van de Ven, T. G. M., *Colloidal Hydrodynamics*, Academic, San Diego, Calif., 1989.

Yamashita, R., and H. Kimura, Particle-tracking techniques for nuclide decay chain: Transport in fractured porous media, *J. Nucl. Sci. Technol*., *27*, 1041–1049, 1990.

Zimmerman, R. W., and G. S. Bodvarsson, Hydraulic conductivity of rock fractures, *Transp. Porous Media*, *23*, 1–30, 1996.

C. V. Chrysikopoulos and S. C. James, Department of Civil and Environmental Engineering, University of California, Irvine, CA 92697-2175. (costas@eng.uci.edu)

(Received April 6, 1998; revised October 14, 1998;
accepted October 14, 1998.)